Inter-Chip Wireless Communication Channel: Measurement, Characterization, and Modeling

Zhi Ming Chen, *Student Member, IEEE*, and Y. P. Zhang

***Abstract*—Wireless chip area network (WCAN) that realizes wireless interconnects within a chip (intra-chip) or among chips (inter-chip) represents a new development in wireless communications. WCAN features unique intra- and inter-chip wireless channels. This paper focuses on understanding of inter-chip wireless communication channels in computer cases. Inter-chip wireless communication channel is characterized for the first time based on measurements conducted in frequency domain inside a computer case on a laboratory workbench. A novel technique for doubling the time-domain resolution is proposed for converting the frequency-domain data to time-domain using inverse discrete Fourier transform (IDFT). It is found that path loss factor is 1.607 for case closed and energy follows lognormal distribution in small scale. Based on analysis in practical situations, channel models are developed and simulated. Comparison between model-generated and empirical data shows that simulated channel responses closely match experimental data. Further more, sampled data in different computer cases give consistent results, making the work presented a representative channel model for wireless inter-chip communication.**

***Index Terms*—Channel modeling, wireless chip-area network, wireless interconnect.**

I. Introduction

FOR THE PAST few decades, performance of integrated circuit (IC) has mainly depended on device properties. In order to enhance circuit and system performance, the major effort has been focused on improving the device speed through scaling of device feature dimension. The down-scaling of device dimension has led to operating speed and cutoff frequency (f_t and $f_{\max}$) exceeding 100 GHz and at the same time the proportional reduction in interconnect cross-sectional area and pitch together with via size [1].

Metal wiring method has been adopted for traditional interconnect technology. The decrease in physical dimension of hard-wired metal interconnects hurts circuit and system performance seriously, especially at high operating frequencies, e.g., interconnect resistance, capacitance, inductance and bit-rate capacity. The associated parasitic capacitance and inductance increase the time delay (*RC* or *LC*). Signal attenuation and dispersion in wire resulted from scaling give arise to degraded bit-rate capacity whose upper bound is $\sim 10^{16}A/l^2$ (or $\sim 10^{17}A/l^2$ by equalizing channels) [2], where A and l are the cross-sectional area and the length of the interconnect wire respectively. Other issues such as *IR* voltage drop, CV^2f power loss and crosstalk between wires become significant as well.

To circumvent the problems in interconnect caused by down-scaling of device feature dimension, a great amount of work has been focused on improving the interconnect performance by reducing the interconnect resistivity (using copper) or reducing the dielectric constant of the interlayer material (using low-κ polymer). However, these approaches will encounter the fundamental material limit sooner or later, to which no known solution exists currently. Therefore, to conquer the obstacle in the evolution of deep submicron ultra large scale integration (ULSI) technology, revolutionary approaches must be pursued. Three different approaches have been attempted: three-dimensional integration, optical links, and wireless interconnect [3]–[5]. As only wireless interconnects are compatible with the mainstream system-on-chip and system-in-package technologies for low-cost system production, they have drawn considerable attention recently. For example, Floyd *et al.*have developed on-chip antennas, integrated transmitters and receivers for wireless interconnects [6]. Zhang has proposed the WCAN concept using impulse or ultrawide-band (UWB) radio as its physical layer to save circuitry overhead and power consumption [7]–[9]. It is seen that some work has been done in the design of on-chip antennas and circuits for wireless interconnects or WCAN applications [8]–[10]. However, little work has been done to understand the wireless communication channel within a chip or among chips. To realize WCAN over intra- or inter- chip channels, it is essential to have knowledge of the channel. Therefore, we focus on understanding of inter-chip wireless communication channels in this paper. Radio propagation channel within a computer case as practical situation is characterized for both casing closed and open conditions. Models are extracted and simulated for the inter-chip wireless communication channel. Simulated responses are compared with empirical data, showing that generated channel responses closely match experimental data in the practical situation. Measurements in different computer cases give consistent channel parameters. Therefore, the channel presented is for typical wireless inter-chip communication.

The paper is organized as follows. In Section II, experiment background, equipment and procedures are described. Data processing and parameter extraction using best fit procedures are presented in Section III. In Section IV, channel models have been implemented based on the parameters derived, and simulation results of the implemented model are compared with experimental data. Finally, conclusions are drawn in Section V.

Manuscript received June 23, 2006; revised September 26, 2006.

The authors are with the School of Electrical and Electronic Engineering, Nanyang Technological University, Singapore 639798, Singapore (e-mail: chen0185@ntu.edu.sg; eypzhang@ntu.edu.sg).

Digital Object Identifier 10.1109/TAP.2007.891861

II. UWB Inter-Chip Channel Measurement

A. Background

Channel measurement can be performed in either frequency domain [11], [12] or time domain [13]. A comparison for characterizing UWB channel using the two techniques has been given in [14]. Because of the Fourier transform relationship between channel impulse response and channel transfer function in frequency domain, data measured using a vector network analyzer (VNA) can be converted to time domain using IDFT. Being a swept frequency technique, high measurement dynamic range is readily obtainable. The generic system is relatively flexible since the frequency of operation, multipath resolution and maximum measurable delay can be reconfigured by adjusting the operation parameters of the VNA. Further more, since the VNA system operates with a transmitted reference, it provides a power delay profile (PDP) with an absolute delay. This technique has been proven as accurate as many time domain techniques when long distance measurement is not required [12]. For interested readers, a detailed description of utilizing VNA for wideband channel measurement has been provided in [15].

The time domain resolution is $1/\mathrm{B}$ in complex baseband approach [11], where B is the measured frequency range. However, by making use of properties of discrete Fourier transformation (DFT) and IDFT, the time domain resolution can be increased up to $1/2\mathrm{B}$. For a $2\mathrm{N}+1$-point finite length discrete-time signal $x[n]$, $n = 0, 1, 2, \ldots, 2\mathrm{N}$, DFT is given by $X[k] = \sum_{n=0}^{2N} x[n] e^{-j2\pi(k/2N+1)n}$, where $k = 0, 1, 2, \ldots, 2\mathrm{N}$. DFT of $x[n]$ is $2\mathrm{N}+1$-point periodic. The frequency domain signal has magnitude response as an even function and phase response as an odd function. If a VNA is used to record the frequency response of the $2\mathrm{N}+1$ discrete time signal $x[n]$, only $\mathrm{N}+1$ frequency points can be observed, which corresponds to $k = 0$ to Nyquist component ($k = \mathrm{N}$) of the sequence $X[k]$. If the discrete-time domain signal is reconstructed based on the $\mathrm{N}+1$ points frequency response, the time domain data becomes $\mathrm{N}+1$ points, yet still covers the same time span as the original discrete time signal $x[n]$, which has $2\mathrm{N}+1$ points. Therefore, the time-domain resolution becomes half of the original discrete time signal. To prevent this loss of the time domain resolution, the obtained $\mathrm{N}+1$ frequency response is extended into $2\mathrm{N}+1$-point by reconstructing components above $k = \mathrm{N}$.

IDFT can be applied together with various windows. A rectangle window gives time domain resolution as $1/2\mathrm{B}$ while hamming window leads to a worse resolution $1.37/2\mathrm{B}$. On the other hand, rectangle and hamming windows result in 13.3 dB and 42.5 dB sidelobe attenuations respectively. To get the best time domain resolution, rectangle window is applied during IDFT to sampled frequency domain data, while attenuation of 13.3 dB is sufficient for suppression of sidelobes.

B. Equipment

Antenna is a critical component for characterizing the inter-chip wireless channel. To sample inter-chip channel, a pair of UWB antennas [16] is used, whose measured impedance bandwidth is shown in Fig. 1. The adopted UWB antenna has S11 lower than -10 dB over 6.7 GHz from 3.75 to 10.45 GHz.

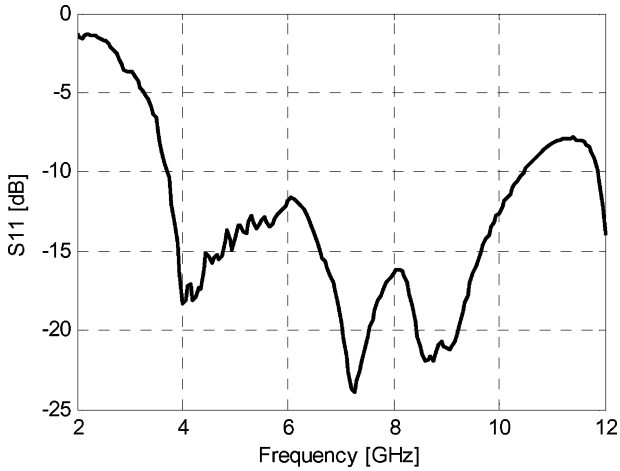

Fig. 1. Measured S11 of UWB antenna over frequency.

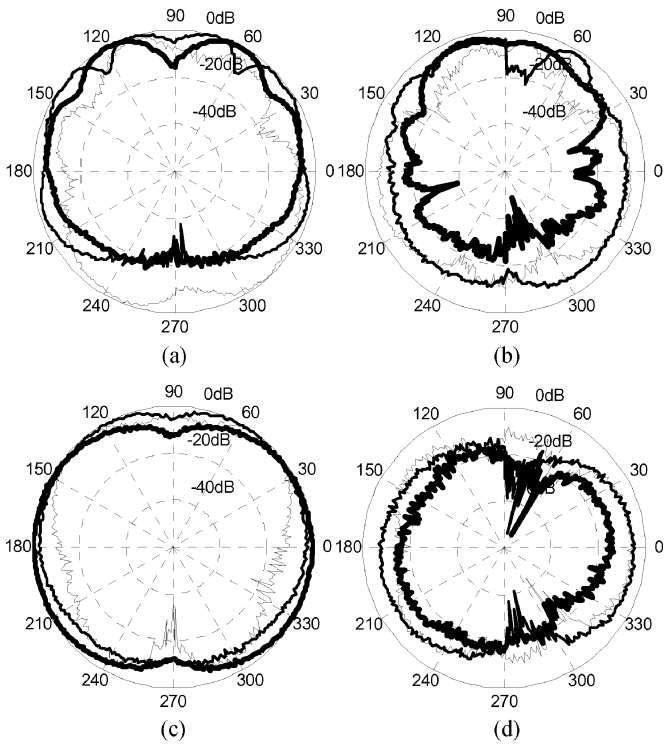

Fig. 2. UWB antenna radiation patterns: (a) and (b) E plane co- and cross-polarization respectively; (c) and (d) H plane co- and cross- polarization respectively. Thick, normal and thin lines are for frequencies 3.5, 6.85 and 10.0 GHz respectively in each plot.

Measured radiation patterns of UWB antenna in both E and H planes are depicted in Fig. 2 for frequencies 3.5, 6.85 and 10 GHz. It can be observed that the UWB antennas display quasi omni-directional patterns.

In addition to impedance bandwidth and radiation patterns, normalized transfer function and group delay are given in Fig. 3, where the measured S21 is normalized to the standard antenna to calibrate the range related effect [17]. The transmitting and receiving antennas are placed in a face-to-face co-planar orientation with a separation distance of 1.6 meters. A dual-polarized quad-ridged horn antenna WJ-48430 is chosen as a standard antenna, which has been proved well matched to the measurement

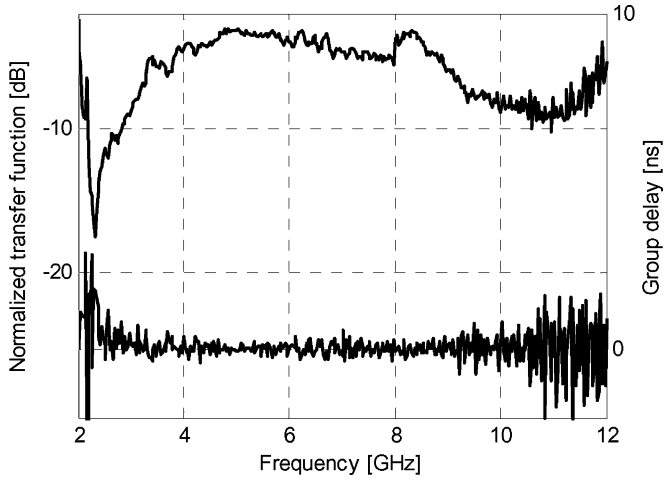

Fig. 3. UWB antenna normalized transfer function and group delay. Top, normalized transfer function; bottom, group delay.

system from 3 to 18 GHz. A relatively flat gain and nearly constant group delays can be observed over the band of interest.

Time domain performance of the UWB antenna has been checked against distortion with the fourth derivative of a Gaussian pulse with $T = 175$ ps

$$p(t) = \left[3 - 6\left(\frac{4\pi}{T^2}\right)t^2 + \left(\frac{4\pi}{T^2}\right)^2 t^4\right] e^{-2\pi(t/T)^2} \quad (1)$$

and a modulated pulse with $f_c = 5$ GHz and $\alpha = 300$ ps

$$p(t) = \sin(2\pi f_c t) e^{-(t/\alpha)^2}. \quad (2)$$

Both pulses comply with FCC indoor emission mask for UWB. Fidelity factor [16] is used to evaluate pulse distortions introduced by antennas and a unity fidelity factor indicates no distortion. The UWB antenna has high fidelity factors of 0.98 and 0.9958 for Gaussian fourth derivative and the modulated pulses respectively.

In the measurement of inter-chip channel within a computer case, it is found difficult to place antenna close to chip surface as large-area chips are not readily available and there are many surrounding discrete components. Therefore, a pair of UWB antennas described above is placed vertically using a right angle connector. In order to sound the channel in the computer case, two 20 cm semi-flexible cables are inserted between antennas and network analyzer cables.

The network analyzer used for recording is an Agilent PNA-L network analyzer of model N5230A up to 20 GHz. Data collection is performed in a typical commercial COMPAQ personal computer, where components such as independent graphic card, memory, hard drive, floppy drive and zip drive are installed. Measurement setup is shown in Fig. 4 and a photograph is given in Fig. 5.

C. Procedures

To measure WCAN channel in a computer case, the sampling points on the motherboard are shown in Fig. 6, where labeled points correspond to the snapshot in Fig. 5. During measurement, no object is moving around. Further more, for closed

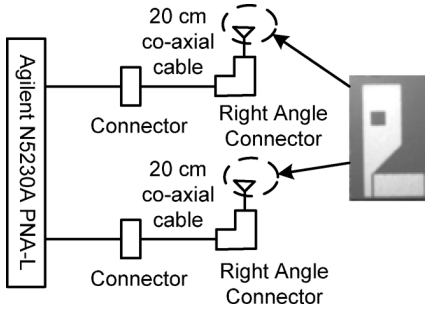

Fig. 4. Measurement setup for channel in a computer case.

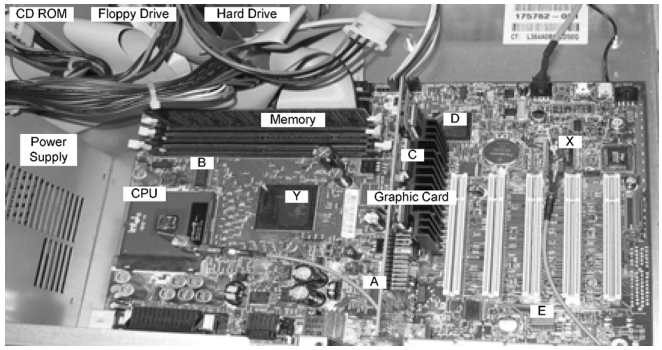

Fig. 5. Measurement snapshot.

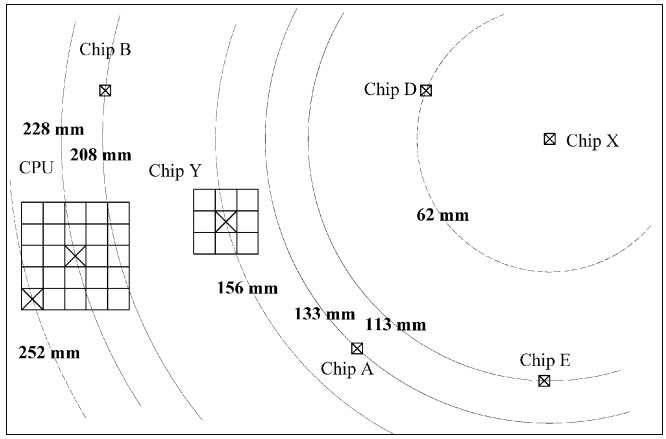

Fig. 6. Measurement points on motherboard.

computer case, the enclosure are well shielded against external interferences. Therefore, the multipath channel can be considered frozen or quasi-static [18]. Heatsink and CPU fan are removed for the convenience of measurement. There are four series of measurement. Series B places transmitting and receiving antennae on Chip X and grids of CPU respectively. In Series C, receiving antenna is placed on grids of Chip Y while transmitting antenna remains on Chip X. For both series B and C, line of sight (LOS) path is blocked by the graphic card inside of the case. In series D, transmitting antenna is placed on the top right grid of Chip Y and receiving antenna moves on the grids of CPU. Series E has six measurement configurations: Chip X-A, B, memory, C, D and E. Chip C is on the standing graphic card and is not shown in Fig. 6. Sampling frequency range is chosen as 3.1–10.6 GHz to obtain the highest allowable emitting power

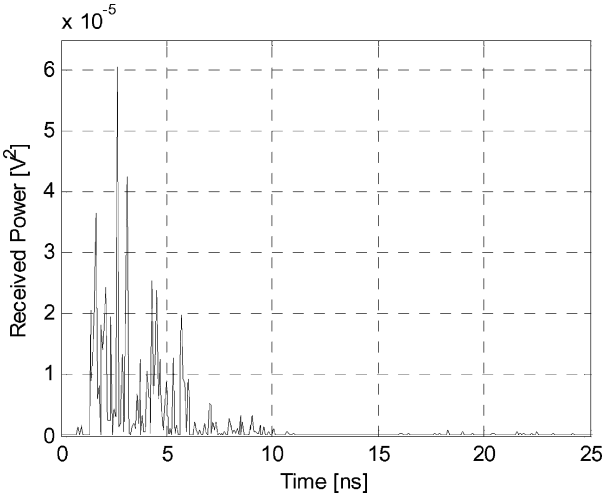

Fig. 7. NLOS received power for computer case closed.

under FCC regulations. For all recorded data in channel measurement, the computer case is placed on work bench in a typical laboratory and recording is performed for both computer case closed and open. Full two-port calibration has been performed up to right-angle connector tips.

III. Data Processing and Results Analysis

Surrounding environment, such as PCI card, chips, discrete components, wires, metal case etc., results in transmitted signal taking multipath to the receiver. Hence signals arriving at the receiver get attenuated, delayed and phase-shifted differently. Impulse response can be presented mathematically by

$$r(t,\tau;d) = \sum_{k=1}^{N_{bins}} a_k(t;d)\exp(j\theta_k(t;d))\delta(t-\tau_k) \qquad (3)$$

where d is the T-R separation distance, N_{bins} is the number of multipath components, a_k is the amplitude, θ_k is the associated phase and τ_k is the excess delay of k^{th} path relative to the first arrival. δ is the Dirac delta function. Multipath power delay profile (PDP) in time domain of (3) is converted from recorded frequency response using IDFT. Delay axis is quantized into bins [19]. Since two multipath components arriving within a bin cannot be resolved, the bin size $\Delta\tau$ is generally chosen to be the resolution of the specific measurement. For measurement in a computer case, the bin size is 66.6667 ps. To reduce observation noise, energy in each bin below certain threshold is set to zero. The threshold is set to 10 dB above noise floor, which is determined by average received noise. The noise floor is determined from the segment of 15 to 20 ns as the energy decays almost completely around 10 ns. Fig. 7 gives a typical NLOS received power when computer case is closed.

For inter-chip channel characterization, statistic parameters for large scale and small scale are analyzed separately. The large scale fading characterizes the changes in the received signal when the transmitter-receiver distance changes significantly or the position and/or environment of the transmitter changes [19]. For WCAN measurement, large scale is defined as when transmitter is fixed on one chip, and receiver moves on another chip. PDP averaged over local area is denoted as small-scale average PDP (SSA-PDP) to determine global parameters. On the other hand, small-scale fading characterizes the changes in the received signal when the changes of positions of transmitter or receiver are not significant. Hence, moving receiving antenna on grids of the same chip gives small scale data, which are used to extract local parameters. Inter-chip wireless communication within a computer case is close to practical situations. Details of channel modeling and analysis are given in the parts below.

TABLE I
Path Loss Parameters

	Case closed	Case open
γ	1.607	2.692
d_0 (mm)	62	62
PL_0 (dB)	23.78	25.27
σ (dB)	0.5482	1.9088

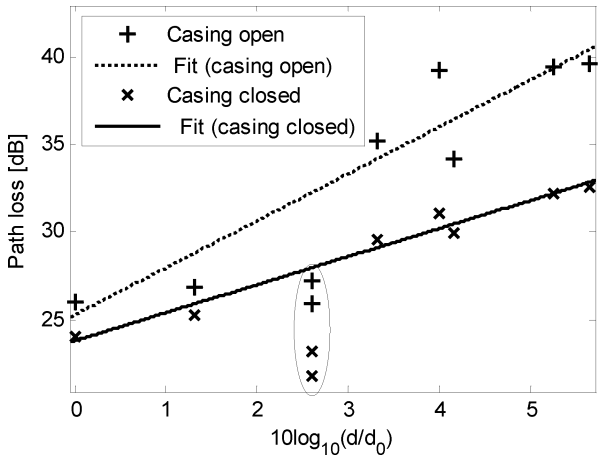

Fig. 8. Path loss fitting of inter-chip channel.

A. Large Scale Analysis

Path loss factor is an important parameter for large scale modeling and can be extracted from SSA-PDPs. Path loss factor determines the average received power over distance. Path loss model [19] can be described by

$$PL = \gamma 10\log_{10}\left(\frac{d}{d_0}\right) + PL_0 + X_\sigma. \qquad (4)$$

PL is the path loss, which gives power attenuation in dB at distance d. d_0 is the reference distance. PL_0 is the interception of model fitted line with vertical power loss axis. γ is the power loss factor. The factor X_σ is a zero mean Gaussian distributed random variable (in dB) with standard deviation σ [19]. By fitting the data to the above models with confidence level 95%, parameters for path loss model can be extracted as given in Table I

Fittings of path loss scatter plot are depicted in Fig. 8. During WCAN sampling, there are discrete components in close proximity of antennas such that antenna characteristics are altered more or less. As a result, antenna effect cannot be calibrated out from sampled inter-chip channel response. Rich multipath in the computer case does change path loss factor. When the computer case is closed, most energy bounces inside of the case, leading to a small path loss factor and low power attenuation. However,

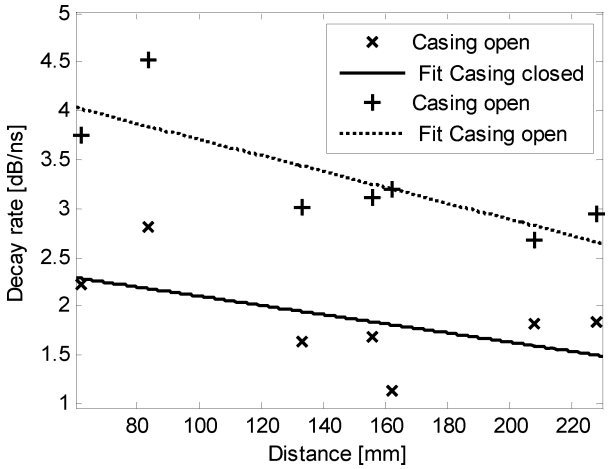

Fig. 9. Decay rates over distance.

when case is open, a significant portion of energy escapes out of the case and the remaining portion still gets reflected and attenuated, giving a higher power loss and path loss factor. The difference in path loss between case closed and case open increases when T-R distance increases. Another important phenomenon is antenna to metal cover distance. When antenna is too close (7 mm) to metal case, either surrounding or ceiling metal cover, much lower power attenuation than that for other situation is observed. This is clearly shown in Fig. 8 by the data points in an ellipse. These points are excluded during fitting since antenna is supposed to keep certain distance from metal casing to avoid reactive coupling and short circuit. It could be due the fact that energy reflected from metal cover is collected before it scatters out. From the standard deviation of the shadowing effect, it can be seen that closed computer case gives a more uniform environment, leading to a smaller shadowing effect.

In the derivation of path loss parameters, the average PDPs have been derived for series B, C, and D. For series E, individual profile is taken to model the decay rate ε. The averaged PDP of series B, C, and D are fitted into exponential law to obtain the power decay rate. It is found that for series B, C and D, the decay rate of the averaged PDP is very close to the average decay rate for individual PDPs and the decay rates have around 10% deviation from the respective mean values. Therefore an amount of 10% deviation should be included for simulation since the decay rates for series E are obtained from their individual PDPs. The change of power decay rate over distance, shown in Fig. 9, is described by (5)

$$\varepsilon = m \times d + \varepsilon_0 \tag{5}$$

where m, d, and ε_0 are the slope, T-R distance in mm and decay rate at zero interception distance respectively. Parameters for decay rates over distance are summarized in Table II.

From Fig. 9, it can be seen that decay rate is higher when case is open than that for closed case, i.e., energy decays faster when case is open. It is due to the fact that closed case allows signal to bounce more times before it decays completely. Negative values of m indicate that when T-R distance increases, signal has more

TABLE II
PARAMETERS FOR DECAY RATES OVER DISTANCE

	m (dB/ns/mm)	ε_0 (dB/ns)
Case closed	-0.0044721	2.576
Case open	-0.008199	4.528

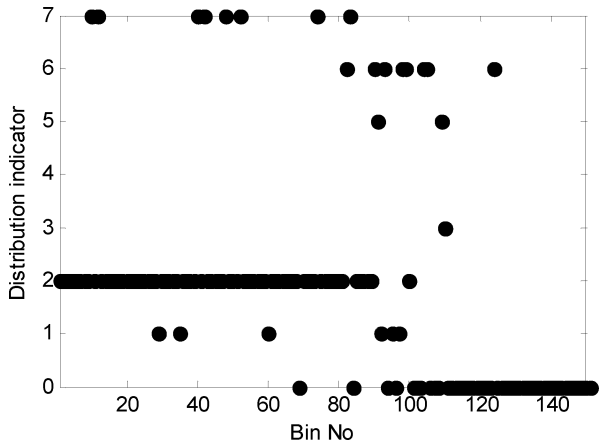

Fig. 10. Small scale distribution of inter-chip channel, case closed.

paths to arrive at the receiving antenna, resulting in a lower time decay rate. A steeper slope for case open shows that the increase in the number of paths in proportion to T-R distance is more important for case open. For closed case, there are a lot of paths even for short distance due to the closed environment; therefore, the increase in number of paths due to increase in T-R distance is not as critical as that when case is open.

B. Small Scale Analysis

Variations of energy amongst grids of chips are investigated in small scale analysis. Energy of each bin in small scale is fitted into distributions using best fit procedures. Seven distributions are used to fit measurement data, including gamma, lognormal, Nakagami-m, normal, Rayleigh, Rician and Weibull distributions. For lognormal distribution, the power in each bin has been converted into log scale, i.e., $P_{dB} = 10\log_{10}(P)$ and fitted to a normal distribution later on. For Nakagami-m distribution, the maximum likelihood estimator (MLE) is from [20], where psi function $\psi(m)$ is taken as the second order approximation of its asymptotic expansion. For the K-parameter of the Rician distribution, moment-based estimator from [21] is used. All other parameter estimations are based on the methods provided in MATLAB 6.5 documentation [22].

Fitted distributions of each bin are shown in the Fig. 10 for inter-chip wireless channel when computer case is closed. The horizontal axis is the number of bins and the vertical axis indicates the distribution for the corresponding bins. From 1 to 7, distributions are gamma, lognormal, Nakagami-m, normal, Rayleigh, Rician and Weibull distributions respectively. The position zero indicates that energy in that particular bin is lower than the threshold value, which is 10 dB above the noise floor.

It can be observed that from bin 1 to bin 90, lognormal distribution is the best fitting results. From bin 90 onwards, the energy is negligible. Therefore, small scale modeling for case closed is

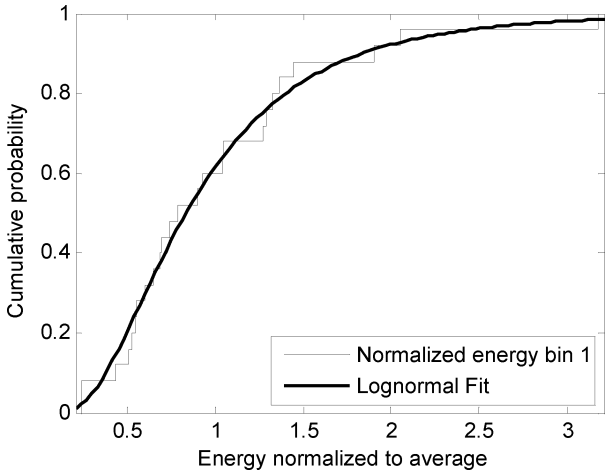

Fig. 11. Fitting of first bin into lognormal distribution, case closed.

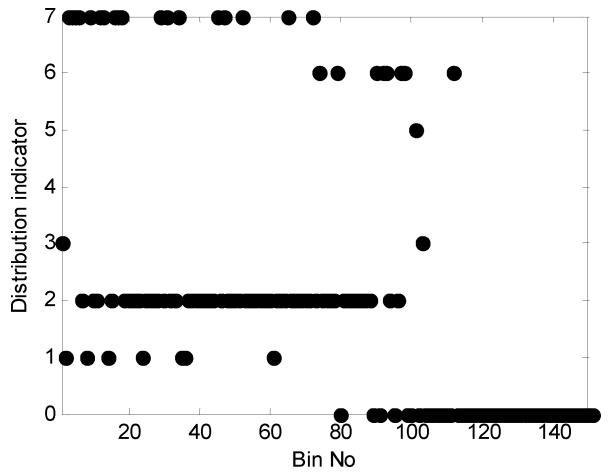

Fig. 12. Small scale distributions, case open.

lognormal distribution up to bin 90. Fitting into lognormal distribution of the first bin is shown in Fig. 11 as an illustration.

Best fitting results for case open is given in Fig. 12. It can be seen that first few bins follow Weibull and normal distributions and afterwards, lognormal distribution is the best fitting. However, by observing the sum of squares due to errors (SSE), it is found that for the first few bins, lognormal still gives a good fitting quality even though it is not the optimum fitting. Small scale distribution for bin 1 is given in Fig. 13 for case open as an example.

As a result, for both case closed and open, lognormal is taken as the small scale distribution up to bin 90. Beyond bin 90, it is considered negligible energy exists.

For case closed, fitting of normalized energy into lognormal distribution from bin 1 to bin 90 gives 90 sets of parameters for the lognormal distributions (μ, σ). It is found that μ and σ follows normal distribution as given by Figs. 14 and 15.

Fitting μ into normal distributions gives two parameters μ_μ and σ_μ. The dependency of the two parameters in distance is given by (6) and (7)

$$\mu\_\mu = 0.009741 \times d - 2.313 \tag{6}$$

$$\sigma\_\mu = -0.004473 \times d + 1.909. \tag{7}$$

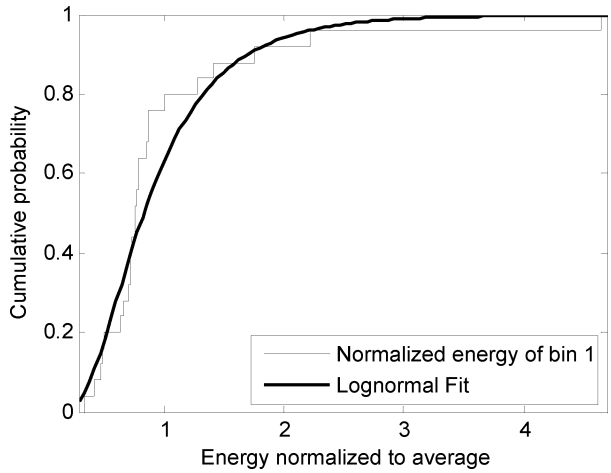

Fig. 13. Fitting of first bin into lognormal distribution, case open.

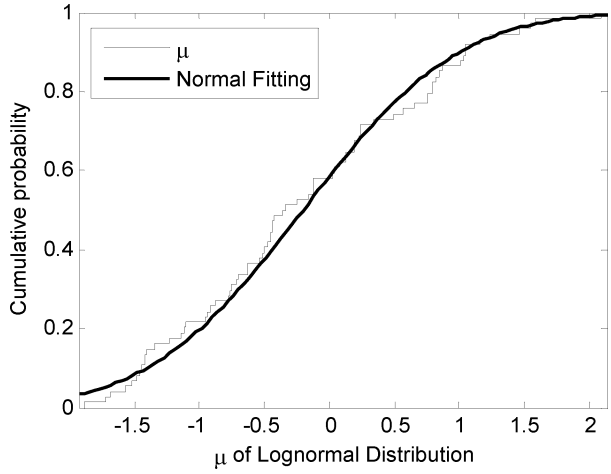

Fig. 14. Fitting of μ into normal distribution, case closed.

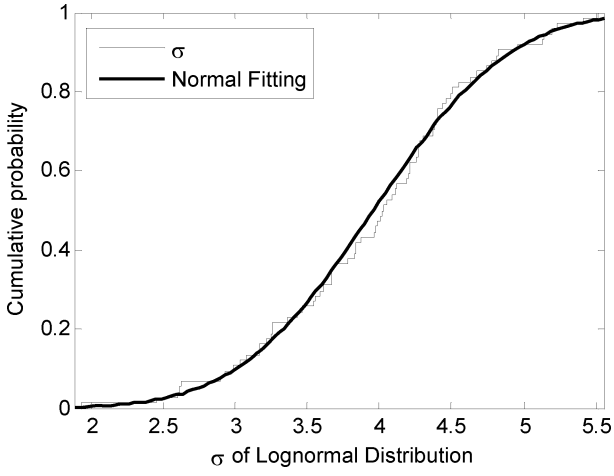

Fig. 15. Fitting of σ into normal distribution, case closed.

Similarly, fitting σ into normal distributions gives another two parameters μ_σ and σ_σ, which are distance dependent as described by (8) and (9)

$$\mu\_\sigma = -0.006687 \times d + 5.239 \tag{8}$$

$$\sigma\_\sigma = -0.003702 \times d + 1.631. \tag{9}$$

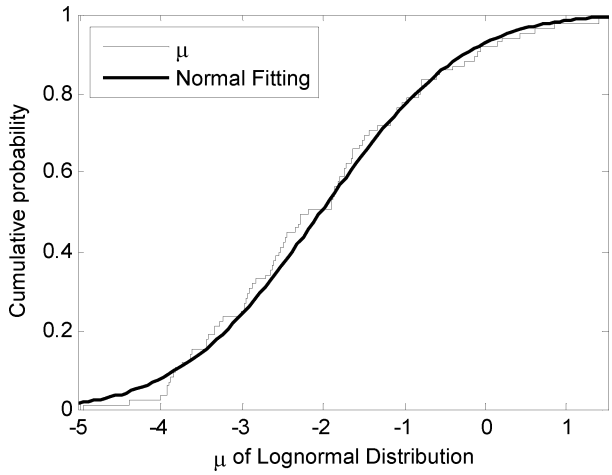

Fig. 16. Fitting of μ into normal distribution, case open.

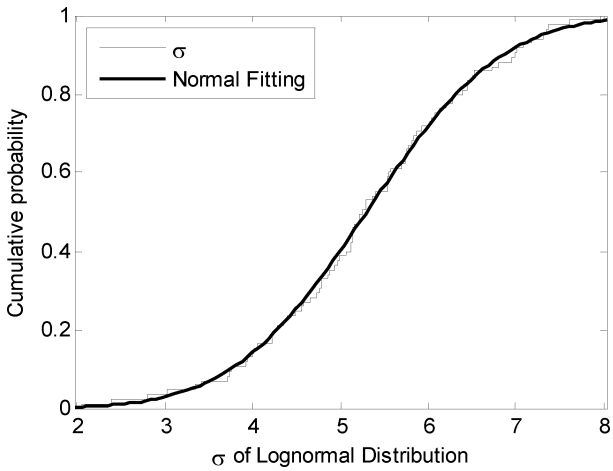

Fig. 17. Fitting of σ into normal distribution, case open.

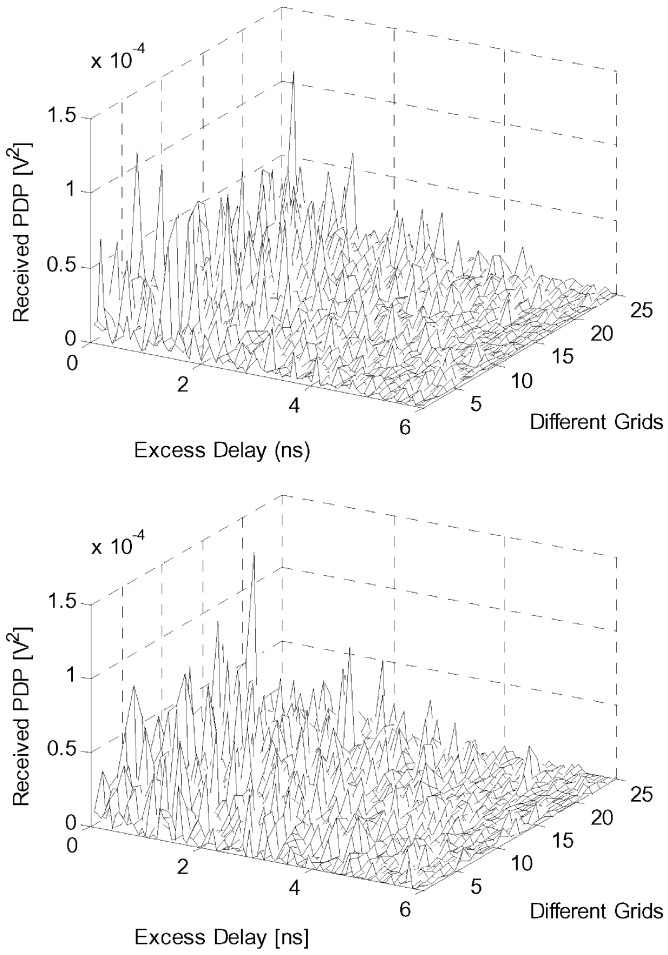

Fig. 18. (a) Generated small scale PDPs for case closed. (b) Experimental small scale PDPs for case closed.

Similarly when the computer case is open, small scale distribution of energy in each bin follows lognormal distribution: $L_N(\mu, \sigma)$. Parameter σ for different bins gives normal distribution by parameters μ_μ and σ_μ as shown in Fig. 16. Variation of the two parameters over distance is described by (10) and (11). The standard deviation of the lognormal distribution gives another normal distribution as given in Fig. 17. The normal distribution parameters μ_σ and σ_σ changes over distance as described by (12) and (13)

$$\mu\_\mu = -0.00219 \times d - 1.405 \tag{10}$$

$$\sigma\_\mu = -0.003338 \times d + 2.12 \tag{11}$$

$$\mu\_\sigma = 0.002901 \times d + 4.244 \tag{12}$$

$$\sigma\_\sigma = -0.005302 \times d + 2.872. \tag{13}$$

IV. Model Implementation, Simulation and Verification

The inter-chip wireless channel is generated according to parameters extracted in the Section III. Given certain distance, total power attenuation *PL* can be generated according to (4) and parameters of γ, d_0, PL_0, σ given in Table I. *PL* is converted into linear scale to obtain power ratio r. Decay rate ε is generated from (5) and parameters in Table II. SSA-PDPs can be generated with power ratio r and decay constant ε. The observation window length is set to 90 bins with bin width the same as measurement resolution. For inter-chip channel, (6)–(13) give lognormal distribution parameters, which can be used to generate individual PDPs for both case closed and open. Fig. 18 gives the comparison of small scale PDPs for computer case closed.

From the comparison, it can be seen intuitively that the model-generated results closely match the experimental data. Quantitative comparison between measured and simulated CDF (fitted using normal distribution) of received power is shown in Fig. 19 for a distance of 84 mm and available LOS signal. The received power is obtained by lumping energy over all bins for each local PDP [13].

The modeling makes sense if the experimental data is sampled in a typical environment for wireless inter-chip channel. Sampled data from a Ranger WorkHorse commercial computer denoted as series K are used for comparison. The Ranger WorkHorse personal computer have independent graphic card, memory, hard drive, floppy drive and zip drive installed. During measurement series K, the CPU heatsink and fan were not removed to make it a practical scenario. The measurement distance covers the range from 43 to 218 mm. Analysis shows that series K has path loss close to value predicted by (4) within

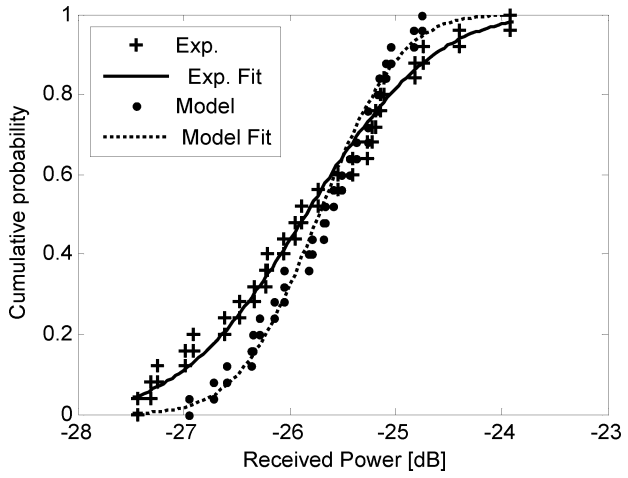

Fig. 19. Comparison between experimental and generated CDF of received power.

2 and 5 dB for case closed and open respectively. Besides, series K indicates that low path loss is obtained when receiving antenna is close to metal case, as mentioned above. Further more, when the T-R distance is too short (43 mm), the path loss model cannot predict received power since the antennas are not in each other's far field. It is found that delay spread in series K is within the range of measurement series B to E, too.

V. Conclusion

Statistical analyses of inter-chip wireless channel have been performed from the data obtained from extensive measurement on PCB inside computer cases, which is a practical situation for inter-chip wireless channel. Based on the parameters extracted, statistical models were implemented for computer simulation. Channel measurement in computer case has been performed for different computers.

In practical situations, path loss factors are 1.607 and 2.692 for case closed and open respectively. Closed case gives a lower path loss than freespace and more uniform environment than open case. In small scale analysis, energy distribution has the lognormal as the best distribution in practical situations. Parameters of lognormal distributions follow normal distributions for different bins.

The statistical model implementation has been performed. Simulation results from the implemented models are close to experimental data. Further more, sampled data from different computer cases show the channel parameters are similar though internal structure and case size differ. To our knowledge, this is the first inter-chip modeling based on statistical analysis in practical situations. With inter-chip wireless communication channel of this work, accurate performance prediction of WCAN for inter-chip wireless communication becomes feasible.

Acknowledgment

The authors would like to thank Ms. M. Sun for development and providing data of the UWB antenna.

References

[1] Int. Technology Roadmap for Semiconductor 2004.
[2] M. F. Chang, V. P. Roychowdhury, L. Zhang, H. Shin, and Y. Qian, "RF/wireless interconnect for inter- and intra-chip communications," *Proc. IEEE*, vol. 89, pp. 456–4661, Apr. 2001.
[3] K. Banerjee, S. J. Souri, P. Kapur, and K. C. Saraswat, "3-D ICs: A novel chip design for improving deep-submicrometer interconnect performance and systems-on-chip integration," *Proc. IEEE*, vol. 89, pp. 602–633, May 2001.
[4] D. A. B. Miller, "Rationale and challenges for optical interconnects to electronic chip," *Proc. IEEE*, vol. 88, pp. 728–749, Jun. 2000.
[5] R. H. Havemann and J. A. Hutchby, "High-performance interconnects: An integration overview," *Proc. IEEE*, vol. 89, pp. 586–601, May 2001.
[6] B. A. Floyd, C.-M. Hung, and K. K. O, "Intra-chip wireless interconnect for clock distribution implemented with integrated antenna, receiver, and transmitters," *IEEE J. Solid-State Circuits*, vol. 37, no. 5, pp. 543–552, May 2002.
[7] Y. P. Zhang, "Bit-error-rate performance of intra-chip wireless interconnect systems," *IEEE Comm. Lett.*, vol. 8, no. 1, pp. 39–41, Jan. 2004.
[8] ——, "Wireless chip area network: A new paradigm for antennas, RF(MM)ICs, and communications," in *Proc. IEEE Asia-Pacific Microwave Conf.*, India, 2004.
[9] M. Sun and Y. P. Zhang, "Performance of inter-chip RF-interconnect using CPW, capacitive coupler and UWB transceiver," *IEEE Trans. Microw. Theory Tech.*, vol. 53, no. 9, pp. 2650–2655, Sep. 2005.
[10] A. B. M. H. Rashid, S. Watanabe, and T. Kikkawa, "High transmission gain integrated antenna on extremely high resistivity Si for ULSI wireless interconnect," *IEEE Electron Device Lett.*, vol. 23, pp. 731–733, 2002.
[11] L. Rush, C. Prettie, D. Cheung, Q. Li, and M. Ho, Characterization of UWB Propagation from 2 to 8 GHz in a Residential Environment [Online]. Available: www.intel.com
[12] S. S. Ghasemzadeh, R. Jana, C. W. Rice, W. Turin, and Vahid, "Measurement and modeling of an ultra-wide bandwidth indoor channel," *IEEE Trans. Comm.*, vol. 52, no. 10, pp. 1786–1796, Oct. 2004.
[13] D. Cassioli, M. Z. Win, and A. F. Molisch, "The ultra-wide bandwidth indoor channel: From statistical model to simulation," *IEEE J. Select. Areas Comm.*, vol. 20, no. 6, pp. 1247–1257, Aug. 2002.
[14] Z. Iranharten, H. Nikookar, and G. J. M. Janssen, "An overview of ultra wide band indoor channel measurements and modeling," *IEEE Microw. Wireless Compon. Lett.*, vol. 14, no. 8, pp. 386–388, Aug. 2004.
[15] A. M. Street, L. Lukama, and D. J. Edwards, "Use of VNAs for wideband propagation measurements," *Proc. Inst. Elect. Eng. Comm.*, vol. 148, no. 6, pp. 411–415, Dec. 2001.
[16] Y. P. Zhang and M. Sun, "Chip antennas for ultrawideband radios," *IEEE, Trans. Antennas Propag.*, submitted for publication.
[17] T. G. Ma and S. K. Jeng, "Planar miniature tapered-slot-feed annular slow antennas for ultrawide-band radios," *IEEE Trans. Ant. and Propag.*, vol. 53, no. 3, pp. 1194–1202, Mar. 2005.
[18] M. Z. Win, R.-M Frenando, and R. A. Scholts, "Utlra-wide bandwidth (UWB) signal propagation for outdoor wireless communication," *IEEE VTC'97*, vol. 1, pp. 251–255, May 1997.
[19] T. S. Rappaport, *Wireless Communications: Principles and Practice*, 2nd ed. Englewood Cliffs: Prentice Hall, 2001.
[20] J. Cheng and N. C. Beaulieu, "Maximum-likelihood based estimation of the Nakgami m parameter," *IEEE Comm. Lett.*, vol. 5, no. 3, pp. 101–103, Mar. 2001.
[21] A. Adbi, C. Tepedelenliogu, M. Kaveh, and G. Giannakis, "On the estimation of the K parameter for Rice fading distribution," *IEEE Comm. Lett.*, vol. 5, no. 3, pp. 92–94, Mar. 2001.
[22] MATLAB 6.5 Documentation.

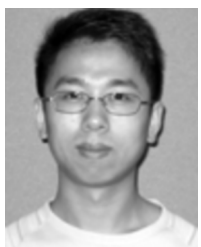

Zhi Ming Chen (S'04) was born in Jiangsu, China, in 1982. He received the B.Eng. degree in electrical and electronic engineering from Nanyang Technological University, Singapore, in 2005, where he is currently working towards the Ph.D. degree in electrical and electronic engineering.

His research interests include study of inter-chip wireless interconnect system and RF transceiver design for wireless communication.

Y. P. Zhang received the B.E. and M.E. degrees from Taiyuan Polytechnic Institute and Shanxi Mining Institute of Taiyuan University of Technology, Shanxi, China, in 1982 and 1987, respectively and the Ph.D. degree from the Chinese University of Hong Kong, Hong Kong, in 1995, all in electronic engineering.

From 1982 to 1984, he was with Shanxi Electronic Industry Bureau. From 1990 to 1992, he was with the University of Liverpool, Liverpool, U.K. From 1996 to 1997, he was with City University of Hong Kong. He taught at Shanxi Mining Institute (1987–1990) and the University of Hong Kong (1997–1998). He was promoted to a Full Professor at Taiyuan University of Technology in 1996. He is now an Associate Professor with the School of Electrical and Electronic Engineering, Nanyang Technological University, Singapore. His research interests include propagation of radio waves, characterization of radio channels, miniaturization of antennas, design of radio-frequency integrated circuits, and implementation of wireless communications systems. He has published widely in the field of radio science and technology across seven IEEE societies. He has delivered scores of invited papers/keynote address at international scientific conferences. He has organized/chaired dozens of technical sessions of international symposia.

Prof. Zhang received the Sino-British Technical Collaboration Award in 1990 for his contribution to the advancement of subsurface radio science and technology. He received the Best Paper Award from the Second International Symposium on Communication Systems, Networks and Digital Signal Processing, 18–20th July 2000, Bournemouth, U.K. He was awarded a William Mong Visiting Fellowship from the University of Hong Kong in 2005. He is listed in *Marquis Who's Who, Who's Who in Science and Engineering, Cambridge IBC 2000 Outstanding Scientists of the 21st Century*. He serves on the Editorial Board of the *International Journal of RF and Microwave Computer-Aided Engineering* and a Guest Editor of the *Journal for the special issue RF and Microwave Subsystem Modules for Wireless Communications*. He also serves on the Editorial Boards of IEEE TRANSACTIONS ON MICROWAVE THEORY AND TECHNIQUES and IEEE MICROWAVE AND WIRELESS COMPONENTS LETTERS.